Methane Monooxygenase Hydroxylase and B Component Interactions†

Jingyan Zhang, Bradley J. Wallar,‡ Codrina V. Popescu,§ Daniel B. Renner, David D. Thomas, and John D. Lipscomb*

Department of Biochemistry, Molecular Biology and Biophysics and Center for Metals in Biocatalysis, University of Minnesota, Minneapolis, Minnesota 55455

Received November 3, 2005; Revised Manuscript Received January 3, 2006

ABSTRACT: The interaction of the soluble methane monooxygenase regulatory component (MMOB) and the active site-bearing hydroxylase component (MMOH) is investigated using spin and fluorescent probes. MMOB from *Methylosinus trichosporium* OB3b is devoid of cysteine. Consequently, site-directed mutagenesis was used to incorporate single cysteine residues, allowing specific placement of the probe molecules. Sixteen MMOB Cys mutants were prepared and labeled with the EPR spin probe 4-maleimido-2,2,6,6-tetramethyl-1-piperidinyloxy (MSL). Spectral evaluation of probe mobility and accessibility to the hydrophilic spin-relaxing agent NiEDDA showed that both properties decrease dramatically for a subset of the spin labels as the complex with MMOH forms, thereby defining the likely interaction surface on MMOB. This surface contains MMOB residue T111 thought to play a role in substrate access into the MMOH active site. The surface also contains several hydrophilic residues and is ringed by charged residues. The surface of MMOB opposite the proposed binding surface is highly charged, consistent with solvent exposure. Probes of both of the disordered N- and C-terminal regions remain highly mobile and exposed to solvent in the MMOH complex. Spin-labeling studies show that residue A62 of MMOB is located in a position where it can be used to monitor MMOH−MMOB complex formation without perturbing the process. Accordingly, steady-state kinetic assays show that it can be changed to Cys (A62C) and labeled with the fluorescent probes 6-bromoacetyl-2-dimethylaminonaphthalene (BADAN) or 5-((((2-iodoacetyl)-amino)ethyl)amino)naphthalene-1-sulfonic acid (1,5-IAEDANS) without loss of the ability of MMOB to promote turnover. The BADAN fluorescence is partially quenched and red shifted as the complex with MMOH forms, allowing affinity measurements. It is shown that the high affinity of labeled MMOB (K_D = 13.5 nM at pH 6.6, 25 °C) for the oxidized MMOH decreases substantially with increasing pH and increasing ionic strength but is nearly unaffected by addition of nonionic detergents. Similarly, the fluorescence anisotropy of the 1,5-IAEDANS-labeled A62C-MMOH complex is perturbed by salts but not nonionic detergents. This suggests that the MMOB−MMOH complex is stabilized by electrostatic interactions consistent with the characteristics of the proposed binding surface. Reduction of MMOH results in a 2−3 order of magnitude decrease in the affinity of the BADAN-labeled A62C-MMOB−MMOH complex, consistent with previous indications of structural change associated with reduction of the active site dinuclear iron cluster. Utilizing BADAN-labeled MMOB, the association and dissociation rate constants for the MMOB−MMOH binding reaction were determined and found to be consistent with a two-step process, possibly involving rapid association followed by a slower conformational change. The latter may be related to the regulation of substrate access into the active site of MMOH.

Methane monooxygenase (MMO)[1] catalyzes the NADH-coupled reaction of methane with O_2 to form methanol and water (*1*):

$$NAD(P)H + H^+ + CH_4 + O_2 \rightarrow NAD(P)^+ + CH_3OH + H_2O$$

The soluble form of MMO (sMMO) has been isolated from several methanotrophs including *Methylosinus trichosporium* OB3b and *Methylococcus capsulatus* (Bath) (*2*−*8*). sMMO consists of three protein components: a 245 kDa hydroxylase (MMOH) with a $(\alpha\beta\gamma)_2$ subunit structure containing a carboxylate- and bis-μ-hydroxo-bridged dinuclear iron center in each protomer, a 38 kDa reductase (MMOR) containing

† This work was supported by National Institutes of Health (NIH) Grants GM-40466 (to J.D.L.) and AR-32961 (to D.D.T.). B.J.W. was supported in part by NIH Training Grant GM-07323. C.V.P. was supported in part by NIH Postdoctoral Grant F32 GM65698.

* To whom correspondence should be addressed. E-mail: lipsc001@umn.edu. Telephone: (612) 625-6454. Fax: (612) 624-5121.

‡ Current address: Department of Chemistry, Grand Valley State University, Allendale, MI 49401.

§ Current address: Department of Chemistry, Ursinus College, Collegeville, PA 19426.

[1] Abbreviations: MMO, methane monooxygenase; sMMO, soluble form of MMO; MMOH, sMMO hydroxylase; $MMOH_{sites}$, MMOH active sites (2 $MMOH_{sites}$ = 1 MMOH); MMOB, sMMO component B; WT-MMOB, wild-type MMOB; MMOR, sMMO reductase; MOPS, 3-morpholinopropanesulfonic acid; O, P*, P, Q, and T, intermediates from the MMOH catalytic cycle; $MMOH^{red}$, diferrous form of MMOH; $MMOH^{ox}$, diferric form of MMOH; BADAN, 6-bromoacetyl-2-dimethylaminonaphthalene; 1,5-IAEDANS, 5-((((2-iodoacetyl)amino)-ethyl)amino)naphthalene-1-sulfonic acid; TCEP, tris(2-carboxyethyl)-phosphine hydrochloride; MSL spin label, 4-maleimido-2,2,6,6-tetramethyl-1-piperidinyloxy; SDSL, site-directed spin labeling; RRT, reciprocal relaxation time.

10.1021/bi052256t CCC: $33.50
Published on Web 02/07/2006

FAD and a [2Fe-2S] cluster, and a 15 kDa regulatory component (MMOB). MMOH is responsible for O_2 activation at the diiron cluster and subsequent hydrocarbon oxidation (*4*, *9*). The X-ray crystal structure of MMOH has been solved and shows that the diiron cluster is bound in the α-subunit approximately 12 Å below the protein surface in a cavity with no obvious access route to bulk solution (*10*, *11*). This contrasts sharply with the structure of other diiron cluster containing oxygenase enzymes, such as Δ^9-stearoyl-acyl carrier protein desaturase and toluene monooxygenase, in which large substrate access channels exist (*12*−*14*).

sMMO employs a complex regulatory system in order to ensure that NADH utilization is tightly coupled to hydrocarbon oxidation and that, once oxygen is activated, it reacts preferentially with methane. This latter aspect of regulation is important because methane is the only physiologically relevant substrate of methanotrophic bacteria. Nevertheless, designing a system to preferentially oxidize methane is nontrivial because it has the highest bond dissociation energy of any linear hydrocarbon, and it has none of the common shape, polarity, and charge determinants normally used by biological systems to ensure specificity. The regulatory system of sMMO is implemented via a collaboration between MMOH and MMOB. Previous studies have revealed the very significant impact that MMOB has on catalysis (*5*). For example, product distribution studies show that MMOB controls the regioselectivity of hydroxylation of complex alternative substrates, suggesting that it can control the shape of the MMOH active site (*15*). Also, the redox potential of MMOH is 132 mV lower when it forms a complex with MMOB, suggesting that the environment of the MMOH dinuclear iron cluster is altered as MMOB associates with MMOH. Accordingly, EPR (*4*, *16*, *17*) and CD/MCD (*18*) studies have shown that the spectroscopic properties of the cluster are substantially altered when the complex with MMOB is formed.

Some insight into the basis for these and many other effects of MMOB has been gained through structural and kinetic studies. Cross-linking studies showed that MMOB forms a specific complex with the α-subunit of MMOH (*16*). Rapid freeze−quench studies showed that the rate constant for the reaction of diferrous MMOH with O_2 to form the first peroxo (or superoxo) intermediate P* is increased 1000-fold by formation of the MMOB−MMOH complex. This shifts the rate-limiting step from the beginning of the catalytic cycle to the end, allowing at least four additional intermediates (P*, P, Q, and T) to be directly detected (*9*, *19*−*21*). The NMR structure of MMOB has been solved and shows that it has both a well-folded core section and extended, disordered N- and C-terminal regions (residues 1−35 and 127−138, respectively) (*22*−*24*). NMR relaxation studies showed that residues from both the core and disordered regions of MMOB interact with MMOH in the complex (*23*, *24*). Mutation of these residues either singly or in small groups was shown to alter the rate constants of specific steps in the catalytic cycle (*25*). In particular, mutation of a cluster of four residues N107G/S109A/S110A/T111A (termed the Quad mutant) to smaller, more hydrophobic residues causes the reactive intermediate Q to transfer oxygen to large substrates more rapidly and the product complex T to release large products more efficiently. This observation led to the suggestion that a major function of MMOB is to create a pathway of some sort into the buried active site of MMOH small enough to allow only methane and O_2 easy passage, providing a very straightforward method for selection.

The "molecular sieve" mechanism of selection by MMO has been tested in several ways. One test was based on the observation that the exceptionally large deuterium kinetic isotope effect on the reaction of methane with intermediate Q [KIE ≈ 50 (*26*)] was not observed when ethane was used as an alternative substrate (*27*). This would be expected if ethane is too large to enter the active site rapidly, making binding rate limiting instead of C−H bond breaking. Use of the Quad mutant of MMOB, or its functional derivative, MMOB-T111A, in place of MMOB unmasked an ethane KIE of ∼2, presumably due to a "widening" of the access pathway by reducing the size of the MMOB residues at the portal.

The next step in understanding the physical basis for the MMOB−MMOH regulatory system is to structurally characterize the complex and its interface surface. Unfortunately, cocrystallization of these two sMMO components has not been achieved, and the complex is too large for NMR solution structures. On the basis of the X-ray crystal structure of MMOH, it has been suggested that the MMOB docks in a "canyon" created by the interface of the two protomeric trimer units (*10*). EPR (*28*) and mass spectroscopic analysis of cross-linked components (*29*) have suggested that the binding occurs on the surface of the MMOH α-subunit that faces the canyon. No studies to date have definitively identified the specific amino acid side chains that compose the binding surface of either MMOH or MMOB.

Here we apply the techniques of site-directed spin labeling (SDSL) (*30*) and small metal chelate paramagnetic relaxation (*31*) to assess the change in mobility and accessibility of specific spin-labeled MMOB residues upon complex formation with MMOH. Both techniques identify a single binding surface, which includes the residues of the Quad mutant. This information is used to identify a site away from the binding interface that can be labeled with fluorophores to allow a detailed investigation of the thermodynamics and kinetics of complex formation as well as the stabilizing forces of the component interface. This study lends new insight into the critical structural factors that lead to regulation of monooxygenase catalysis in the sMMO system and the roles of residues that serve to gate substrate access.

EXPERIMENTAL PROCEDURES

Reagents. Common reagents were of the highest grade available and were obtained from either Sigma (St. Louis, MO) or Aldrich Chemicals (Milwaukee, WI). They were used without further purification. Reagents for cloning, mutagenesis, and overexpression were purchased from Promega (Madison, WI), New England Biolabs (Beverly, MA), Life Technologies Inc. (Rockville, MD), Stratagene (La Jolla, CA), Invitrogen (Carlsbad, CA), and Qiagen (Valencia, CA). The sulfhydryl-specific probes, 6-bromoacetyl-2-dimethylaminonaphthalene (BADAN) and 5-((((2-iodoacetyl)amino)ethyl)amino)naphthalene-1-sulfonic acid (1,5-IAEDANS), and 4-maleimido-2,2,6,6-tetramethyl-1-piperidinyloxy (MSL), as well as the reducing agent, tris-(2-carboxyethyl)phosphine hydrochloride (TCEP), were sup-

plied by Molecular Probes, Inc. (Eugene, OR). DEAE-Sepharose and Sephadex G-25, G-50, and G-75 resins were products of Pharmacia (Piscataway, NJ). Water was deionized and further purified using a Millipore reverse osmosis system.

Bacterial Growth and Protein Purification. MMOH and MMOR were purified from *Ms. trichosporium* OB3b, and enzyme and protein assays were conducted as previously reported (*4*, *32*). MMOB was purified after overexpression in *Escherichia coli* as previously described (*22*, *25*), but a modified refolding method was used (*46*). The total yield was approximately 200 mg of refolded MMOB from 20 g wet weight of recombinant *E. coli* for expression of both WT-MMOB and its mutant forms.

Site-Directed Mutagenesis. All of the site-directed mutations were made in the pBWJ400 plasmid (*25*) containing the WT-MMOB gene using a QuikChange kit (Stratagene, La Jolla, CA). All of the mutations were confirmed by sequencing at the University of Minnesota Microchemical Facility. The oligonucleotides used to introduce the mutations to the MMOB gene are shown in Table S1 (see Supporting Information). The mutant MMOBs were expressed and purified as described above for WT-MMOB.

Steady-State Kinetic Measurements. Steady-state kinetic experiments were performed using a Hewlett-Packard 8453 UV−vis spectrophotometer. For the multiple turnover reaction with the substrate nitrobenzene, the reaction rates were monitored by the release of the product *p*-nitrophenol at 404 nm ($\epsilon = 15\ mM^{-1}\ cm^{-1}$) or the consumption of NADH at 340 nm ($\epsilon = 6.24\ mM^{-1}\ cm^{-1}$) in 50 mM MOPS buffer, pH 7.6 at 25 °C. The maximum activity of the mutants was determined by keeping all other reaction components fixed while varying the MMOB concentration. In some cases, comparative studies were performed by measuring O_2 uptake using a Clark-type oxygen electrode and furan as the assay substrate.

Site-Directed Labeling. The purified MMOB or mutant MMOB was diluted to 100 μM final concentration in anaerobic 50 mM MOPS, pH 7.0. A 10-fold molar excess of TCEP [tris(2-carboxyethyl)phosphine] was added to reduce any disulfide bonds between MMOB molecules, and the reaction was allowed to proceed for 2 h under Ar. To prepare spin-labeled samples, a concentrated MSL stock solution was prepared in DMSO, and a small amount was added to the protein solution to give a final concentration of 1 mM. The labeling reaction was complete in 2 h at room temperature or overnight at 4 °C. An excess of mercaptoethanol or cysteine was then added to consume excess MSL. The labeled MMOB was purified by extensive dialysis at 4 °C with 25 mM MOPS, pH 7.0.

To prepare BADAN-labeled A62C, a small amount of BADAN stock solution (50 mM stock in DMF) was added to the TCEP-reduced A62C to give a 200 μM final solution, and the mixture was allowed to stir under anaerobic conditions at 4 °C for 2.5 h. For the 1,5-IAEDANS labeling, 1,5-IAEDANS (75 mM stock in DMF) was added to 200 μM final concentration, and the mixture was allowed to stir at 4 °C for 20 h. In each case, the reaction was quenched by addition of 500 μM cysteine. The reaction mixtures were dialyzed versus 2 L of 50 mM MOPS, pH 7.0, for 3 h (3×). After dialysis, labeled protein was further purified on a Sephadex G-25 column. The final sample was frozen with liquid nitrogen and stored at −80 °C.

To quantitate the extent of BADAN and 1,5-IAEDANS labeling, a standard curve was first generated for both dyes in solution after reaction with cysteine. The concentration of the dye could be determined from the 394 nm (BADAN) or 340 nm (1,5-IAEDANS) absorbance value alone. However, both BADAN and 1,5-IAEDANS absorb in the 280 nm region, complicating protein determinations. Consequently, the dye concentration was used to correct the 280 nm absorbance for the contribution of the fluorophore, allowing an accurate protein concentration to be determined. In all cases, the ratio of both BADAN and 1,5-IAEDANS to A62C was 1.0 ± 0.05.

Circular Dichroism Spectroscopy. CD measurements were performed on a Jasco 710 spectropolarimeter at room temperature in the range of 190−260 nm. Protein samples (100 μM) were prepared in 25 mM MOPS, pH 7.0. Final spectra are the averages of six scans.

EPR Spectroscopy. EPR spectra were acquired by using a Bruker EleXsys 500 spectrometer with the SHQ cavity. Samples were measured in quartz capillaries at 25 °C set by using a Bruker temperature controller. All spectra were obtained with a 100 G scan width, using 100 kHz field modulation with an amplitude of 2 G. Power saturation curves were obtained by monitoring the peak-to-peak intensity of the central resonance ($m_I = 0$) as a function of incident microwave power. Typically, the MMOB concentration was lower than 100 μM, and the total volume was 25 μL. All the EPR samples were prepared in 50 mM MOPS buffer, pH 7.0.

Accessibility Measurement. Solvent accessibility of the spin label was determined by use of the hydrophilic paramagnetic relaxing agent nickel ethylenediaminediacetic acetate (NiEDDA), which was synthesized according to an established procedure (*33*). This reagent increases the relaxation rate by collisional spin exchange, so the microwave power required for half-saturation increases in proportion to solvent accessibility (*31*, *34*). The EPR signal in the presence and absence of 3 mM NiEDDA was recorded as a function of incident microwave power, and the data set was fit by

$$A = IP^{1/2}[1 + (2^{1/b} - 1)P/P_{1/2}]^{-b} \quad (1)$$

where A is the signal amplitude, I is a scaling factor, P is the incident microwave power, $P_{1/2}$ is the microwave power at half-saturation, and b is a measure of the homogeneity of the saturation line. In the nonlinear least-squares fit, I and $P_{1/2}$ were allowed to vary freely and b was allowed to vary in the range of 0.5−1.5 (*35*). Spectral parameters for the saturation data were fit to eq 1 using Origin 5.0 to obtain $P_{1/2}$.

The increase in $P_{1/2}$, $\Delta P_{1/2}$, due to the relaxing agent, is proportional to the collision frequency W divided by the spin−spin relaxation time, T_2 (*31*, *34*):

$$\Delta P_{1/2} = P_{1/2} - P_{1/2}{}^0 \propto W/T_2 \quad (2)$$

where $P_{1/2}{}^0$ is the microwave power at half-saturation without NiEDDA added. It has been found experimentally that the peak-to-peak width of the central $m_I = 0$ resonance (ΔH) is

proportional to T_2^{-1}, allowing a relative value of W to be determined. A convenient method to compare the accessibility for different labeled sites on MMOB in the presence and absence of MMOH is obtained from the ratio of relative W values (*34*):

$$F = \frac{\Delta P_{1/2}/\Delta H \text{ (with MMOH)}}{\Delta P_{1/2}/\Delta H \text{ (without MMOH)}} \quad (3)$$

Mobility Measurement. The EPR spectrum of the bound spin label offers a very sensitive measure of the mobility of the probe, but this mobility is affected by contributions from many sources, including local probe dynamics, segmental motion of the protein, and the protein correlation time. The EPR spectral line shape is altered as the probe becomes immobilized with the separation of the extrema increasing from about 31.8 G for completely mobile to 70 G for completely immobile on the EPR time scale (nanoseconds) (*36*). The inverse of the central $m_I = 0$ resonance line width (ΔH^{-1}) provides a semiquantitative measurement of the mobility that averages all of the sources of motion (*37*). Normalizing this value to the ΔH^{-1} values for the most (ΔH_m^{-1}) and least (ΔH_i^{-1}) mobile conditions observed for the protein under study provides a convenient method to compare changes in mobility for labeled positions:

$$M = \frac{\Delta H_{obs}^{-1} - \Delta H_i^{-1}}{\Delta H_m^{-1} - \Delta H_i^{-1}} \quad (4)$$

Fluorescence Measurements. All steady-state and time-resolved fluorescence spectroscopy measurements on samples of labeled MMOB or MMOH-MMOB complexes at equilibrium were made at 25 °C using either the SPEX Fluorolog DM3000 (Edison, NJ) or the ISS PC1 and K2 photon counting and multifrequency phase fluorometer (Champaign, IL). In the case of BADAN-A62C MMOB, an excitation wavelength of 394 nm was used, while 490 nm was monitored for emission. For 1,5-IAEDANS-labeled MMOB, 338 nm was used as the excitation wavelength, whereas a 488 nm band-pass filter was used in monitoring the emission of the probe. All stopped-flow emission measurements were performed using an Applied Photophysics Ltd. SX.18MV stopped-flow spectrometer equipped with the SK.1E extended spectra kinetic accessory (Surrey, United Kingdom). All reactions proceeded at 4 °C. An excitation wavelength of 395 nm was used, and emission was monitored using a 455 nm cutoff filter. In the determination of "on" rates for MMOB to MMOH, oxidized MMOH in 50 mM MOPS, variable pH, was rapidly mixed with BADAN-A62C MMOB in the same buffer. For linear and log time traces, 1000 data points were collected. The rate constants are averages of at least 10 experiments, unless otherwise noted.

Calculations. For all of the steady-state fluorescence titrations of MMOH to BADAN-A62C MMOB, the concentration of MMOH is given in active sites, or $MMOH_{sites}$ ($2\ MMOH_{sites} = 1$ MMOH). The best-fit model assumed that the two $\alpha\beta\gamma$ protomers (active sites) are identical and independent of each other; therefore, each MMOH protomer was fit as if a separate protein. No evidence that the two protomers are nonequivalent was observed in the fluorescence titrations. The fraction bound was determined from the fractional change in fluorescence over the maximum change at saturation. This allows the concentration of sites bound and free to be calculated from the known total concentrations of MMOH and MMOB in the mixture. A plot of fraction bound versus [$MMOH_{sites}$] was then fit to the one-site Adair equation by nonlinear regression analysis to yield the K_D value.

For the fluorescence anisotropy experiments using 1,5-IAEDANS-labeled A62C-MMOB, four different measurement conditions were used, V_V, V_H, H_H, and H_V, reflecting the polarization of exciting/monitoring light (e.g., H_V denotes horizontal excitation and vertical detection). Anisotropy (r) was calculated as follows:

$$r = (V_V - GH_V)/(V_V + 2GV_H) \quad \text{where } G = H_V/H_H \quad (5)$$

$$r = r_0(\text{app})/[1 + (\tau_L/\tau_C)] \quad (6)$$

where r_0(app) is the limiting anisotropy in the absence of motion, τ_L is the fluorescence lifetime, and τ_C is the rotational correlation time (*38*).

Table 1: Activities of the Cys Mutants of MMOB

protein	relative activity[a] (% of WT)	MMOB/$MMOH_{site}$ at activity maximum[b]	$MMOH_{site}$/MMOB-MSL[d] at saturation of EPR complex
WT-MMOB	100	1	
R133C	93	1	2
G119C	97	2	4
A115C	107	2 (2)[c]	6
T111C	54	2 (4)[c]	4
S109C	68	2	4
Y102C	88	2 (4)[c]	6
A89C	97	1 (1)[c]	2
D87C	85	1	2
I84C	102	4 (4)[c]	6
D71C	84	1	2
V68C	95	1	2
A62C	95	1 (1)[c]	2
D54C	88	7.5	3
K44C	77	1 (2)[c]	4
V39C	92	1	3
K15C	80	1	2

[a] The details of the activity assay are described in Experimental Procedures. They represent the maximum activity at the optimum MMOB:MMOH ratio for each mutant. [b] The MMOB mutant/$MMOH_{site}$ ratio is the point at which the maximum activity is reached for each mutant. These mutants are not spin-labeled. [c] The MMOB:MMOH ratio for maximum activity for the MSL-labeled mutants was determined in some cases and is shown in parentheses. [d] The amount of MSL spin-labeled MMOB mutant added in the experiments for Figures 1, S2−S4, or 3 to approach saturation of the complex as judged by the EPR spectrum. The value of 2 indicates that saturation was reached between 1:1 and 2:1, and intervening values were not tested.

RESULTS

Cysteine Mutants of MMOB. On the basis of the NMR solution structure of MMOB (*22*), 16 sites were selected for mutagenesis to incorporate single Cys residues into the structure. These positions, listed in Table 1, were selected due to either their surface location, their suggested involvement in binding to MMOH from previous studies (*23*, *28*), or their postulated role in the mechanism of catalysis (*25*, *39*). All structural regions of MMOB were represented, although only about 12% of the total number of MMOB

residues were altered. The cysteine mutants expressed well and did not result in any significant changes in the stability of MMOB.

Steady-State Kinetic Assays. MMOB activity is measured as an enhancement of MMOH turnover activity in the reconstituted sMMO system. WT-MMOB increases the turnover number approximately 150-fold (*4*). As shown in Table 1, all of the mutants can support at least 50% of the wild-type rate with several showing full activity. The rate-limiting step in the MMOH catalytic cycle is usually product release when the form of MMOB used is able to enhance the rate of initial O_2 binding (*9*, *40*). This appears to be the case for all of the mutants in this study. It is possible that some of the fast steps of the catalytic cycle are slowed by the mutants, but this would not be detected by steady-state measurements.

Past studies have shown that a 1:1 WT-MMOB−$MMOH_{sites}$ complex maximizes the steady-state turnover rate, but larger ratios result in a decreased rate due to formation of inhibitory complexes between two MMOB molecules or MMOB and MMOR (*16*). For WT-MMOB, the MMOH complex is very stable such that a 1:1 ratio of components saturates the active complex even at assay concentrations. This is also true for some of the mutant MMOBs, but others require a larger ratio as shown in Table 1. Evidently, mutation to Cys in some positions weakens the MMOB−MMOH complex, perhaps due to inclusion of the Cys residue in the binding interface. When the spin label is added, the mutants retain their activity, although the ratio of MMOB−MMOH that maximizes the activity increases slightly in some cases (Table 1).

CD Measurements. To confirm that the mutations did not affect the structure, far-UV CD spectra were recorded. The spectra of most mutants are indistinguishable from that of WT-MMOB in 190 to 260 nm region. However, the spectra of the three mutants shown in Figure S1, I84C,[2] D54C, and A89C, exhibit some differences in both the 195−200 and 200−225 nm regions, suggesting local reorganization of secondary structure. The NMR structure shows that the I84 and A89 residues extend into the center of the protein structure, and thus it is not unreasonable for their substitution to cause structural modifications (*22*). Residue D54 appears to be on the MMOB surface, but it is in a cluster of Glu and Lys residues. Alteration of the charge in this case may cause a disruption in the MMOB structure. This is consistent with the data shown in Table 1, which indicates that I84C and D54C have a somewhat decreased ability to enhance turnover and lower affinity for MMOH. Although these structural changes do not inactivate MMOB, they may cause a change in the MMOB−MMOH interaction, and thus they will not be considered further in this study.

Spin Label Mobility. The mobility of the MSL spin labels placed in different positions of MMOB varies widely. For example, as shown in Figures 1A and S2, the splitting between the extrema of the spectrum of the R133C-MSL and K15C-MSL, with modified residues located on the disordered C- and N-terminal region, respectively, of MMOB, is approximately 37 G. This is close to the value of 31.8 G observed for MSL freely tumbling in solution (τ_c < 1 ns),

[2] The mutated MMOB is referred to in this study by identifying the site of the mutation.

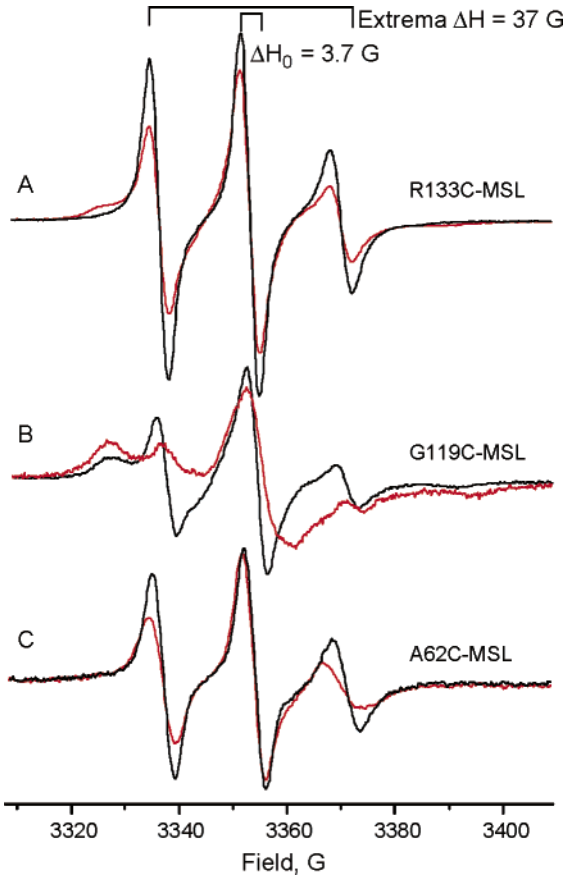

FIGURE 1: EPR spectral changes for labeled MMOB mutants. Representative spectra are shown for spin-labeled MMOB mutants alone (black) and after addition of equimolar $MMOH_{sites}$ (red). Spectra of all of the labeled mutants are shown in Supporting Information, Figures S2−S4. (A) A mutant labeled in the C-terminal region. A similar result is observed when a mutant labeled in the N-terminal region is examined (see Figure S2). (B) A mutant labeled in the putative MMOB−MMOH interface region of the well-folded core structure. (C) A mutant labeled in the region of the well-folded core that is proposed to be solvent-exposed in the MMOB−MMOH complex. For mutants that exhibit a substantial spectral change when MMOH is added, the change is generally not maximized by equimolar $MMOH_{sites}$. The ΔH_0 data shown in Table 2 were determined from the spectra of samples where sufficient $MMOH_{sites}$ was added to maximize the spectral change. Instrumental parameters are given in Experimental Procedures.

thus indicating a correlation time much shorter than the $\tau_c \approx 6$ ns expected for the 15 kDa MMOB itself (*36*). On the other hand, the spectra of several of the modified MMOBs, for example, that of A115C-MSL in Figure 2 (also see Figures 1B and S3), exhibit extrema separated by 64−67 G, similar to the 70 G expected for the MSL spin label immobilized in a solid. Thus, in these cases, the long correlation time suggests that, a significant fraction of the time, the fast local motions of the probe are eliminated, and the probe moves with the entire protein. Most of the labeled residues exhibit motion between these two extremes. In Table 2, the average mobility of the probe is quantified by assigning an *M*-value as described in Experimental Procedures and eq 4. The range of *M*-values is set by the range of mobilities seen for both the free and MMOH-complexed, labeled MMOBs. Most of the *M*-values are in the upper half of the range, suggesting that mobilities of the probes are generally higher when MMOB is not complexed with MMOH, as expected.

Table 2: Mobility and Accessibility Parameters for Spin-Labeled MMOB Mutants Alone and in Complex with MMOH[a]

	MMOB		MMOB−MMOH		MMOB, M_f	MMOB−MMOH, M_b	rel mobility, M_b/M_f	rel access, F
	ΔH_0	$\Delta P_{1/2f}$	ΔH_0	$\Delta P_{1/2b}$				
D87C	6.4[b]	400[c]	6.2[b]	410[c]	0.3	0.3	1.0	1.06
R133C	3.6	350	3.7	320	1.0	1.0	1.0	0.89
K15C	3.6	350	3.7	320	1.0	1.0	1.0	0.88
V68C	3.7	670	3.8	560	1.0	0.9	0.9	0.82
A62C	4.0	350	4.6	320	0.9	0.7	0.8	0.79
K44C	5.4	315	9.8	150	0.5	0	0	0.26
G119C	3.9	190	6.2	50	0.9	0.3	0.3	0.16
S109C	4.9	160	8.7	40	0.6	0.1	0.2	0.15
T111C	3.7	255	5.1	35	1.0	0.5	0.5	0.11
D71C	4.3	190	6.2	30	0.7	0.3	0.4	0.10
V39C	4.3	1070	7.9	205	0.7	0.1	0.1	0.10
A115C	4.5	130	8.0	15	0.7	0.1	0.1	0.07
Y102C	3.8	1510	7.5	195	0.9	0.2	0.2	0.07

[a] Subscripts f and b refer to free and bound states, respectively, for MMOB. Other definitions and methods for determination of parameters are given in Experimental Procedures. [b] The error in ΔH_0 is approximately ±0.1 G. [c] The error in $\Delta P_{1/2}$ is approximately ±5%.

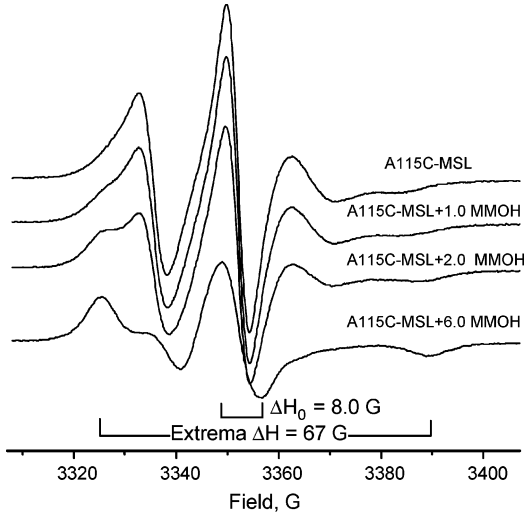

FIGURE 2: EPR spectral changes of A115C-MSL in the presence of MMOH. MMOH was added in the ratio shown to spin-labeled A115C. Instrumental parameters are given in Experimental Procedures.

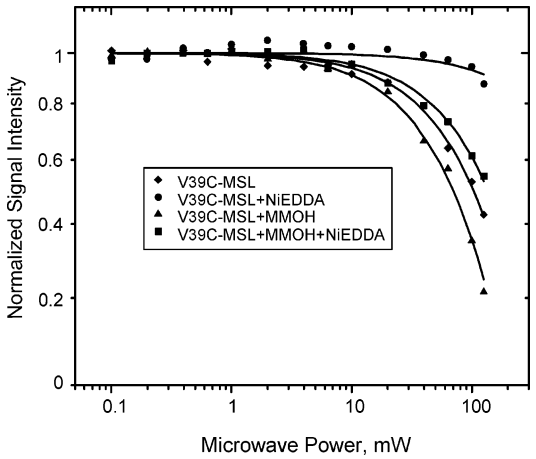

FIGURE 3: Power saturation curves of spin-labeled MMOB in the presence and absence of MMOH and NiEDDA. The microwave saturation curve of MSL spin-labeled MMOB mutant V39C alone and after mixing with 2 equiv of $MMOH_{sites}$ (saturated complex). Then, the measurements were repeated for each sample after addition of 3 mM NiEDDA. Instrumental parameters and data analysis techniques are given in Experimental Procedures.

Addition of MMOH to a concentration sufficient to saturate the MMOB−MMOH complex causes substantial changes in the local probe mobility of some of the labeled MMOB residues. As shown in Figure 2 and Table 2, titration of MMOH into a sample of A115C-MSL causes a very significant shift from high to low mobility. Similarly, each of the labeled residues represented in Figures 1B and S3 shows a substantial restriction in mobility when the complex with MMOH forms even in a 1:1 ratio (also see Table 2 for ΔH_0 values when the complexes are saturated). This is consistent either with these residues forming part of the MMOB−MMOH interface or with a conformational change caused by complex formation that restricts the local motion of the probes.

Two sets of residues show little or no reduction in mobility when the complex forms. The labeled residues in the N- and C-terminal regions continue to move rapidly after MMOH binds, as shown in Figures 1A and S2 and Table 2. Also, as seen in Figures 1C and S4 and Table 2, labeled residues V68C, A62C, and D87C show only slightly altered spectra, and their mobility is changed marginally or not at all.

Spin Label Accessibility. The origin of the decreased mobility for some residues when MMOH is added can be examined to some extent by determining the accessibility of the probe to solvent or, more specifically, a hydrophilic paramagnetic relaxing agent. It is presumed that a spin label that becomes buried in a protein−protein interface will be significantly less accessible to a relaxing agent such as NiEDDA. The change in the relaxation rate of the probe can be monitored by determining the $\Delta P_{1/2}$ value as described in Experimental Procedures and eqs 1 and 2. By comparing $\Delta P_{1/2}$ values in the presence and absence of MMOH, a differential accessibility parameter F (Table 2) can be calculated as described in Experimental Procedures and eq 3.

A typical power saturation curve for a spin-labeled MMOB mutant in the presence and absence of NiEDDA and MMOH is shown in Figure 3. Both the relaxing agent and MMOH strongly affect the observed power saturation value. Table 2 shows the observed F values for each of the mutant MMOBs in the presence of sufficient MMOH to saturate the complex. Several labeled mutants, including D87C, V68C, and A62C from the core region and R133C and K15C from the C- and N-terminal regions, respectively, are highly accessible and show no significant change in accessibility upon addition of MMOH. The other residues examined have

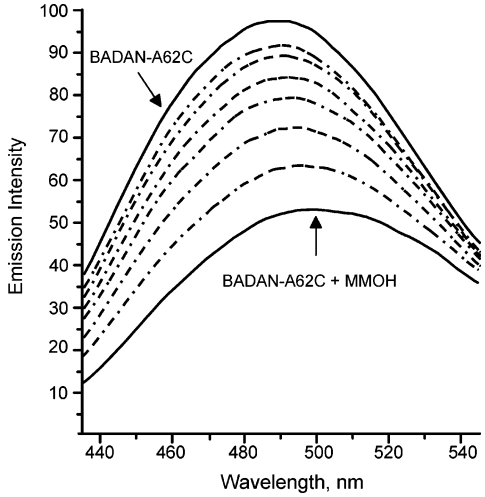

FIGURE 4: The presence of MMOH alters the emission profile of BADAN-A62C, and the effect is reversed by salt. The top emission spectrum is of 200 nM BADAN-A62C alone in 50 mM MOPS, pH 7.0 at 25 °C. The bottom spectrum is observed after the addition of 400 nM $MMOH_{sites}$. After this initial quenching, NaCl was added to final concentrations of 50, 100, 150, 200, 300, and 500 mM (dash-dot lines), resulting in increasing emission intensity. No correction was made for dilution.

varying degrees of accessibility in the absence of MMOH, but they become much less accessible when MMOH is added. The labeled residues are likely to be in the MMOH−MMOB interface, but sequestration by a conformational change in MMOB caused by the formation of the complex cannot be ruled out. It is noteworthy that the spin label of D87C is substantially immobilized both before and after addition of MMOH, yet it is highly accessible to the relaxing agent in both cases. Thus, in this case, the technique can differentiate between immobilization due to the protein structure and that due to formation of the protein−protein complex.

Characterization of the Binding Interface. Inspection of the data in Tables 1 and 2 shows that mutation of the residues at positions 62 or 68 to Cys (i) causes little change in activity, (ii) retains high mobility for bound spin labels after MMOH binding, and (iii) retains high accessibility to a spin relaxing agent in the MMOH−MMOB complex. This suggests that these residues are not directly in the MMOH−MMOB binding interface, and thus labels at these positions could be used as innocent monitors of the binding process. A62C was chosen for further study because both secondary structure predictions and the NMR solution structure (*22*) showed this residue to be exposed on the surface in a β-turn so that it should have few interactions with other MMOB residues.

BADAN-A62C MMOB Binds to MMOH. A62C was labeled stoichiometrically with the fluorescent probe BADAN as described in Experimental Procedures. Evaluation of the steady-state kinetics for the reconstituted sMMO system and of the transient kinetics of the MMOH single turnover cycle in the presence of BADAN-A62C showed no significant differences from those using wild-type MMOB (Figure S5A). Specifically, the labeled protein maximizes steady-state turnover at a 1:1 ratio with MMOH, showing that a high-affinity complex is formed. Also, it allows formation of the key transient intermediate Q of the reaction cycle at the same rate as WT-MMOB (Figure S5B), suggesting that the oxygen activation phase of the catalytic cycle is not significantly altered.

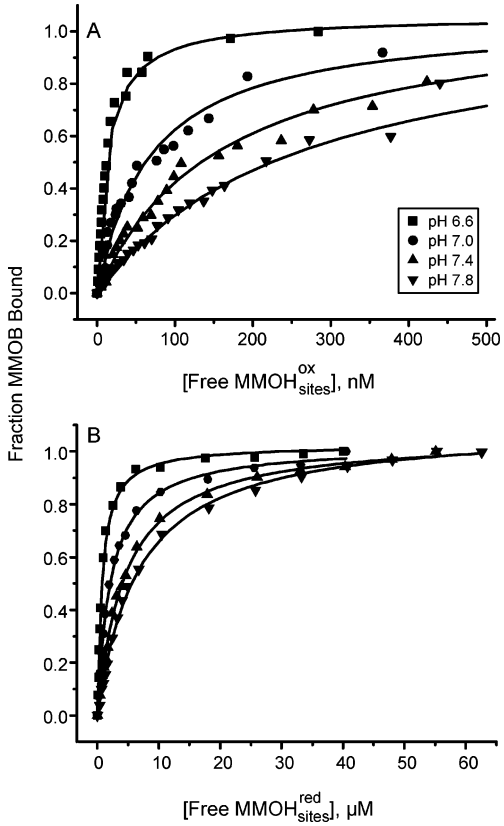

FIGURE 5: MMOH binding to BADAN-A62C. (A) The emission intensity at 490 nm was measured for a sample of 200 nM BADAN-A62C in 50 mM MOPS at the pH values shown at 25 °C. MMOH was added and the fluorescence emission spectrum measured after equilibration. The buffer solution at each pH value was adjusted to equal conductivity, and the excitation wavelength for all measurements was 394 nm. The data for each titration were fit best with a one-site binding model and with the K_D values listed in Table 3. (B) The titration was repeated under anaerobic conditions using MMOH reduced by equimolar sodium dithionite using 1 μM methyl viologen as a mediator.

As shown in Figure 4 (solid lines), the emission profile of BADAN decreases in intensity and shifts to the red as MMOH is added, in accord with our preliminary studies (*29*). This result shows that the environment of the probe is not completely unaltered when the complex is formed. However, the observed changes suggest that it shifts to a more polar environment in the complex (*41*, *42*). Thus, it is unlikely to be a part of the binding interface, in accord with the activity and spin-labeling studies reported above. The observation that BADAN-A62C senses complex formation but does not affect the kinetics of the reaction cycle justifies its selection as a probe of the binding process.

Dissociation Constant for the MMOH−MMOB Complex. Figure 5A shows titrations of a constant concentration of BADAN-A62C MMOB with diferric MMOH at several pH values at constant conductivity. Very good hyperbolic fits to the data are obtained under the assumptions that there is one MMOB binding site per MMOH active site and that there is no cooperativity for MMOB binding between the two active sites in the MMOH dimeric protomer. The K_D values obtained at different pH values are summarized in Table 3. It can be seen from these values that increasing pH causes a decrease in the affinity between MMOH and

Table 3: Equilibrium and Rate Constants for MMOH Binding to BADAN-A62C MMOB

	pH 6.6	pH 7.0	pH 7.4	pH 7.8
K_D (nM),[a] $MMOH^{ox}$	13.5 ± 0.8	68.0 ± 5.3	159.0 ± 9.3	266.0 ± 17.6
K_D (nM),[a] $MMOH^{red}$	770 ± 60	2200 ± 130	4510 ± 310	6690 ± 430
k_1 (M^{-1} s^{-1})[b]	(9.8 ± 0.7) × 10^7	(8.1 ± 0.9) × 10^7	(4.6 ± 0.8) × 10^7	(1.3 ± 0.3) × 10^7
k_{-1} (s^{-1})[b]	1.5 ± 0.7	2.4 ± 0.6	1.9 ± 0.8	3.4 ± 0.8
RRT2 (s^{-1})[b]	13.2 ± 2.1	13.5 ± 2.6	12.6 ± 3.3	14.1 ± 3.9

[a] The dissociation constants were measured at 25 °C to allow comparisons with values determined from fitting steady-state data. [b] The rate constants were measured at 4 °C. MMOH was in the diferric form in all samples. Analysis of the kinetic data yield two RRTs that can be attributed to the binding reaction. Under the assumption that the two RRTs arise from a two-step reaction and that the association step is fast, the faster RRT can be analyzed to yield k_1 and k_{-1} as shown in Figure 8.

MMOB. It should also be noted that the K_D value of 68.2 nM at pH 7.0 is in very good agreement with an earlier study of component interactions in MMO, in which it was assumed that a 1:1 complex between MMOH and MMOB is required for maximum steady-state rate. Numerical integration-based simulations of this model yield the solid lines in Figure S5A and a K_D value of 67 nM for the MMOH−MMOB complex (*16*).

Electrostatic Interactions Play a Role in MMOH−MMOB Binding. To determine whether the stabilization of the MMOH and MMOB complex is due to hydrophobic or hydrophilic forces, the effect of NaCl on the emission profile of the BADAN-A62C MMOB−MMOH complex was evaluated. As shown in Figure 4 (dash-dot lines), the addition of as little as 50 mM NaCl is observed to blue shift and increase the intensity of the emission spectrum. At 500 mM NaCl the emission spectrum of the BADAN-A62C MMOB alone is nearly restored, suggesting that the complex is dissociated. Similar results were observed using KI (data not shown), showing that the effect is not ion dependent and underscoring the conclusion that ionic interactions are likely to be very important in stabilizing the MMOH−MMOB interface. Accordingly, nonionic detergents, including 0.9% *n*-octyl *β*-D-glucopyranoside, 0.1% Tween 20, and 0.1% Triton X-100 had no significant effect on the fluorescence emission spectrum of the BADAN-A62C−MMOH complex.

Fluorescence Anisotropy Studies. Changes in the polarization of fluorophores attached to MMOB can also be used to monitor complex formation and dissociation due to the large difference in Stokes radius of MMOB and the MMOB−MMOH complex. In this case, A62C was labeled with the fluorophore 1,5-IAEDANS because it has a relatively long fluorescence lifetime (10−20 ns), allowing more accurate monitoring of the protein rotation (*38*, *43*, *44*). The addition of MMOH to 1,5-IAEDANS-A62C caused a predictable increase in the overall fluorescence anisotropy due to the increase in the rotational correlation time of the larger MMOB−MMOH complex (τ_C; see Experimental Procedures, eqs 5 and 6, and Figure 6). The presence of detergents again had no significant effect on the degree of fluorescence polarization. Conversely, the addition of NaCl caused the anisotropy to increase much more slowly with added MMOH, showing that the affinity of MMOB and MMOH is substantially decreased. It should be noted that the maximum anisotropy ($r = 0.103$) was the same for salt- or detergent-containing solutions. As a control for the possibility that the fluorescence lifetime of 1,5-IAEDANS might change under the various conditions of this experiment, the lifetime of the probe conjugated to A62C in the uncomplexed form was measured. No change was observed in the presence of salt or detergent, and the lifetime was also unaltered by the presence of excess MMOH (data not shown). The measured lifetime of 12.5 ns agrees with measurements from past studies of 1,5-IAEDANS (*43*, *44*). Therefore, the change in anisotropy upon MMOH addition most likely arises from the increased global molecular weight of the MMOB−MMOH complex and is a valid probe of the MMOB−MMOH binding reaction.

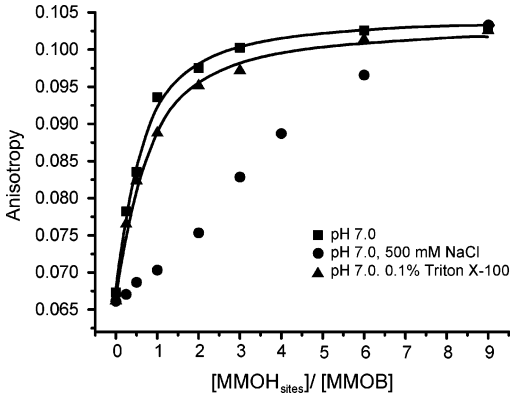

FIGURE 6: Fluorescence anisotropy measurements of MMOH binding to 1,5-IAEDANS-A62C. For each incremental addition of MMOH, the emission intensity at 488 ± 10 nm (band-pass filter) was measured for 1 μM 1,5-IAEDANS-A62C under three experimental conditions: 50 mM MOPS, pH 7.0 (■), 50 mM MOPS, pH 7.0, and 500 mM NaCl (●), and 50 mM MOPS, pH 7.0, and 0.1% Triton X-100 (▲). The data for 0.1% Tween 20 gave the same results as 0.1% Triton X-100. The intensity values were an average of 15 acquisitions, and the anisotropy was calculated for each condition using eq 5. The excitation wavelength for all measurements was 338 nm.

Determination of Rate Constants for the MMOB−$MMOH_{sites}$ Binding Reaction. Using BADAN-A62C, the kinetics of MMOB binding to MMOH can be directly observed as a change in the fluorescence emission intensity. In these reactions, 200 nM BADAN-A62C was mixed rapidly with varying higher concentrations of $MMOH_{sites}$ so as to establish pseudo-first-order conditions. Then, the resulting decrease in fluorescence was monitored over time. As in the equilibrium K_D measurements, binding was measured at pH 6.6, 7.0, 7.4, and 7.8. An example of the observed time course and fit is shown in Figure 7. All of the kinetic traces required a summed two-exponential fit to the data plus a correction for the slow photobleaching of the BADAN fluorophore that occurs with or without the other reaction components present. The reciprocal relaxation times (RRTs) or rate constants are listed in Table 3. It was found that the faster RRT is pH dependent and linearly dependent on the concentration of MMOH (Figure 8), whereas the slower RRT appeared to be independent of both MMOH

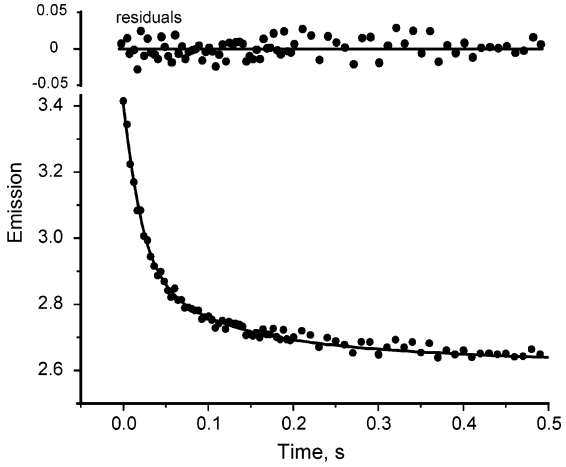

FIGURE 7: Time course of BADAN-A62C MMOB binding to MMOH. 200 nM BADAN-A62C MMOB in 50 mM MOPS, pH 7.0, was rapidly mixed with 2.4 μM $MMOH_{sites}$ in 50 mM MOPS, pH 7.0 at 4 °C (concentrations are before mixing), and the change in fluorescence was recorded. The excitation wavelength and emission collection procedures were the same as described for Figure 5.

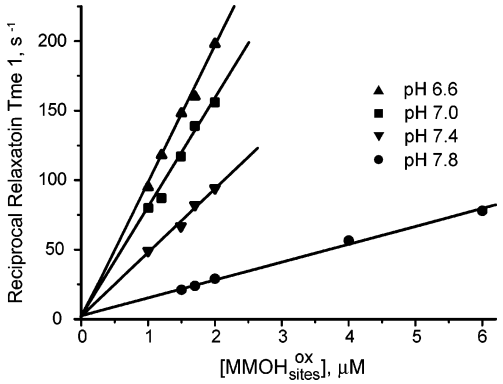

FIGURE 8: Kinetics of MMOB−$MMOH_{sites}$ complex formation. Data such as that shown in Figure 7 were fit to a three summed exponential time course to yield RRT values for each phase. The final phase was independent of the presence of protein and is ascribed to dye photobleaching. As shown here, the fastest of the RRT values for each binding reaction is linearly dependent on the concentration of $MMOH_{sites}$ for all pH values at 4 °C.

concentration and pH. The observation of two kinetic phases could result from a two-step reaction, or there could be two populations of BADAN-A62C or MMOH that react independently at different rates. The two-step reaction hypothesis illustrated below is supported by the lack of concentration dependence in the slower phase, which should easily be observed:

$$\mathrm{MMOH} + \mathrm{MMOB} \underset{k_{-1}}{\overset{\text{association } k_1}{\rightleftharpoons}} \mathrm{MMOB{\cdot}MMOH} \underset{k_{-2}}{\overset{\text{isomerization } k_2}{\rightleftharpoons}} \mathrm{MMOB{-}MMOH}$$

Second-order rate constants were determined for the faster step from the slopes of the lines shown in Figure 8 and are listed in Table 3. All of the plots appear to intercept the RRT axis slightly above the origin, consistent with reverse rate constant of 1−3.5 s^{-1} as listed in Table 3. The high rate of the association step relative to those of the other reactions in the process justifies analyzing it as a single step reaction as is done in Figure 8. The same values for the association rate constant are obtained when the reaction is analyzed as a two-step reversible process by plotting the sum or product of the RRTs versus MMOH concentration (data not shown). The small reverse rate constant for the association in comparison with the RRT for the putative second step (~13 s^{-1}) accounts for the loss of the expected (nonlinear) concentration dependence of the second phase. The values for k_{-1} reported in Table 3 must be considered approximate, because they will become progressively less accurate as the rate of k_2 increases, necessitating analysis as a true two-step reaction. The lack of concentration dependence in the slower phase prevents determination of the reversibility of the second step as well as the individual rate constants, so the observed RRT must be considered as approximately equal to the sum of $k_2 + k_{-2}$. The values for k_1 and k_{-1} reported in Table 3 give calculated values for K_D in the range expected from the direct room temperature determinations reported in Table 3.

DISCUSSION

Past studies have shown that the binding of MMOB and MMOH has remarkable effects on the catalytic process that result in (i) acceleration of the formation of a highly reactive activated oxo species (Q) in a protected environment and (ii) the preferential oxidation of methane over other hydrocarbons with weaker C−H bonds. Little is known about the interface of these two sMMO components. The current study utilizes site-directed spin labeling to probe this interaction and allows the identification of the likely binding surface on MMOB. The characteristics of the proposed surface are then tested against the properties of the actual surface using fluorescent probes placed in a position shown by the spin-labeling study to be unlikely to interfere with the complex formation. Considered together, these studies offer new insight into the nature of the binding surface. This is discussed here in the context of previous structural, binding, and kinetic studies.

Residues in the Binding Surface. The results show that MMOB is a good candidate for SDSL because (i) the overall secondary structure, (ii) the ability to bind strongly to MMOH, and (iii) the specific ability to promote rapid catalysis are all maintained in the labeled mutants. Nevertheless, the environments of specifically labeled sites fall into three distinctly different classes on the basis of changes in the mobility and accessibility of the spin labels.

Labels in the C- and N-terminal regions remain highly accessible and mobile in the MMOH complex. NMR studies indicate that the N-terminal region binds to MMOH (*23*), and catalytic studies show that both the C- and N-terminal regions strongly affect the rate constants of individual steps in the catalytic cycle as well as coupling of reducing equivalents to product formation (*25*, *45*, *46*). However, the current results show that when these regions bind, the labels themselves remain highly mobile and are not tied to the rotation of the MMOB−MMOH complex. Thus, it is likely that the terminal regions do not fold into the core region as the complex forms, because if this occurred, they would probably be shielded from solvent and significantly immobilized.

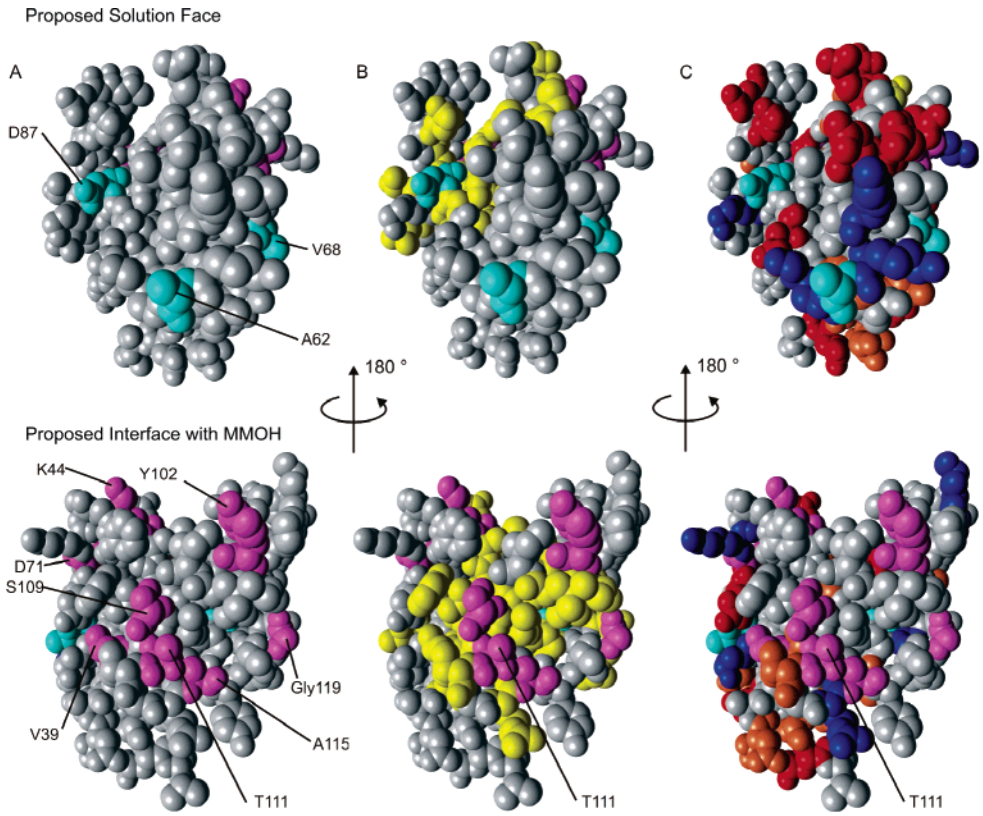

FIGURE 9: Identification and characterization of the MMOB surface that interacts with MMOH. Shown are the proposed solution (top) and MMOH interface (bottom) faces of MMOB. In each section, solvent-exposed residues in the complex are colored cyan while buried residues are colored magenta. (A) Spin-labeled positions only. (B) Compilation of residues proposed to interact with the MMOH from NMR (yellow) (*23*) and spin-labeling studies. Residues indicated by both techniques to be buried are classified with the spin-labeling color code. (C) Compilation of positively (blue) and negatively (red) charged and polar (orange) residues with those proposed to be exposed or buried in the complex by spin-labeling studies.

A second group of labeled residues, including A62C, V68C, and D87C, have varying degrees of mobility, but the mobility and accessibility do not change substantially when MMOH binds. It thus seems likely that these residues are not part of the binding interface. In the past, we have used the ratio of MMOB to $MMOH_{sites}$ that maximizes steady-state turnover as an indication of affinity (*16*). Each of these three mutants shows the same maximized rate at slightly over 1:1 MMOB:MMOH, suggesting that little change occurs in the binding affinity.

The final group of residues, including Y102C, A115C, T111C, D71C, V39C, G119C, S109C, and K44C, are all strongly perturbed in both accessibility and mobility as the MMOH complex forms, suggesting that these residues are either in the interface or in environments that are greatly altered as the complex forms. In contrast to the two groups discussed above, several modified MMOBs in this group exhibit lower affinity for MMOH, as judged by the amount required to maximize steady-state activity as well as the excess required to saturate the change in spin label EPR line shape (listed in Table 1). Previously, we have observed a 10-fold decrease in affinity for the T111Y MMOB mutant, apparently caused in introduction of the larger residue (*39*). The T111 residue is key to gating substrate into the active site and seems likely to be a part of the binding interface. Evidently, the precise interface required for selection between methane and larger hydrocarbons does not readily accept larger residues. This is consistent with the spin-labeled residues in this group forming part of the binding interface.

Figure 9A shows the location of the residues for the second and third groups described above in the NMR solution structure of MMOB. All of the exposed residues based on the spin label study (cyan) are clustered on one face while all of the proposed buried residues (magenta) are on the opposite face. The key residue T111 described above is located in the center of this view of the proposed buried face.

Comparison with NMR Relaxation Studies. NMR has been used both to solve the solution structure of the MMOB component and to evaluate which backbone elements undergo the largest change in relaxation rate when the complex with MMOH forms. This is generally a good indication of which side chains are involved in the interaction but can also report changes in the environment of internal residues. This technique was applied to both the sMMO system from *Ms. trichosporium* OB3b and that from *Mc. capsulatus* (Bath) with similar, but not identical, results. In the application to the *Ms. trichosporium* OB3b (*23*), we noted that it is important to reduce the MMOH for the analysis, because this weakens the binding interaction, as we observed in the studies reported here. This allows more rapid MMOB exchange, providing more reliable data for identification of the binding surface. Figure 9B shows the same two surfaces as in Figure 9A with the residues proposed to be buried from the NMR study colored in yellow. Two residues, V39 and T111, were identified both by NMR and by the present EPR study. The residues detected by the spin label studies are colored in the same way as in Figure 9A. It is clear from this comparison that the techniques identify the same surface.

The fact that side chain interactions are identified by the spin-labeling technique greatly strengthens this assignment.

Characteristics of the Binding Surface. The discussion of the binding surface thus far supports the choice of residue A62 as a position that can be labeled with a fluorescent probe without directly perturbing the binding surface. In fact, the results show that a fluorophore attached to the A62C mutant becomes more exposed to solvent as the complex forms. The intense fluorescence of the BADAN probe greatly simplifies the determination of the K_D values for complex formation. The values obtained for the oxidized enzyme are nearly identical to those we estimated by fitting steady-state kinetic data to a model that requires MMOH−MMOB complex formation to initiate catalysis (*16*). The K_D values have also been determined for the components from the *Mc. capsulatus* (Bath) system using isothermal titration calorimetry (*47*). In that case, the affinity was found to be approximately 4-fold weaker at pH 7.0, 25 °C, but nevertheless in good agreement with the results presented here.

The use of the fluorescent probe has allowed a direct measure of the affinity of reduced MMOH for MMOB for the first time in the current study. The value of 4.5 μM at pH 7.0 shows that the affinity is much weaker than for the oxidized MMOH. This value is again in reasonable agreement with that predicted by modeling the steady-state behavior (26 μM) (*16*). A similar large decrease in affinity was required to model the MMOB concentration dependence of the interconversion of the transient intermediates in the reaction cycle (*40*). Also, we have shown in the past that the redox potential of MMOH decreases by 132 mV when complexed with MMOB, indicative of a large decrease in affinity (*48*).

The results presented here show that the labeled MMOB−MMOH complex is destabilized by relatively low concentrations of salt or by an increase in pH. In contrast, addition of detergents has no effect on the complex stability. This suggests that the binding interface is stabilized by ionic interactions. The opposite conclusion was reached for the *Mc. capsulatus* (Bath) MMOB−MMOH interaction, based on the failure of salt to elute MMOH from a nickel chelate column to which the His-tagged MMOB−MMOH complex had been bound (*49*). However, another research group has shown that masking positively charged residues on MMOH inhibits catalysis in the *Mc. capsulatus* (Bath) sMMO system by preventing MMOB from binding (*50*). Similarly, we have shown that treatment of MMOB in the *Ms. trichosporium* OB3b sMMO system with 1-ethyl-3-(3-(dimethylamino)-propyl)carbodiimide rapidly eliminates its ability to accelerate the reaction by either masking surface carboxylate groups or cross-linking these groups to nearby lysyl residues of MMOB (*16*). Figure 9C shows the position of charged residues (red, Asp, Glu; blue, Arg, Lys) relative to the residues identified as solvent exposed or masked by the spin-labeling study. The putative solvent-exposed surface contains many charged residues as expected. However, the proposed surface that is buried by complex formation also has several charged residues. In this case, they are, for the most part, not in the center of this surface marked by T111 but rather form a ring surrounding the surface. Similar rings of charged residues are often encountered in biological complexes, notably in the cytochrome *c*−cytochrome oxidase complex and the cyt b_5 or putidaredoxin−$P450_{cam}$ interface (*51*, *52*). It should also be noted that the putative interface surface has many uncharged hydrophilic residues (orange in Figure 9C). These include all four of the residues proposed to be active in gating substrate into the MMOH active site, N107, S109, S110, and T111. On the basis of this surface composition, it seems likely that the major stabilizing forces for the complex are ionic and hydrogen bond interactions.

Orientation Relative to MMOH. It is known from cross-linking studies that MMOB binds to the α-subunit of MMOH. The crystal structure of MMOH shows that the boundary between the two $\alpha\beta\gamma$ protomers creates a groove in the structure that is a predictable binding site for MMOB and MMOR (*10*). The MMOH surface facing the groove is also that closest to the buried diiron cluster. On the basis of preliminary cross-linking studies, we have shown that MMOH peptides from this surface, as well as MMOB peptides from the interaction surface proposed here, disappear from tryptic digests when analyzed by mass spectroscopic techniques (*29*). A trial alignment based on these studies shows that the charged residues that surround the putative interface surface have partners on the MMOH surface. However, this alignment is not unique, and programs designed to dock proteins based on structural information show many possible complexes.[3] Additional specific points of interaction will be required to allow a precise model to be constructed.

One study of MMOB from *Mc. capsulatus* (Bath) allowed the determination of a distance of only 15 Å from spin-labeled residue C89 to the diiron cluster of MMOH from that system based on saturation recovery EPR (*28*). The distance from the surface of MMOH to the diiron cluster is at least 12 Å, so this result would imply that MMOB binds on the surface closest to the diiron cluster as proposed above. However, it also implies that the surface we identify as the binding surface in MMOB from *Ms. trichosporium* OB3b is not the binding surface in *Mc. capsulatus* (Bath) MMOB because the equivalent residue in the *Ms. trichosporium* OB3b MMOB (A88) is on the putative solvent-exposed surface. It seems unlikely that the two MMOBs use different binding surfaces because they have nearly the same overall structure. In the results presented here, we have modified and labeled residues A89 and D87. Labeled A89C disrupts the MMOB structure somewhat, and the residue apparently extends into the core structure. Labeled D87C has only moderate mobility, but it is solvent exposed, and this exposure does not change when MMOH is added. The saturation recovery EPR approach can provide precise distance measurements, but precise information about the nature and magnitude of the coupling of the irons in the active site cluster is required for data analysis. A small error in evaluating this coupling could account for the distance discrepancy in the two approaches used to evaluate the MMOH−MMOB interaction.

Comparison of the Putative Binding Surfaces of MMOB Isoforms. A comparison of the aligned amino acid sequences of MMOBs from *Ms. trichosporium* OB3b and *Mc. capsulatus* (Bath) shows overall high sequence identity or similarity. All of the specific residues proposed from this study to form part of the interface with MMOH based on labeling

[3] J. Zhang, B. V. B. Reddy, and J. D. Lipscomb, unpublished observation.

the cysteine replacements are identical in the two forms of MMOB. This suggests that the same surface of MMOB is used in the interface by each system and emphasizes the importance of precise structure in this region. In contrast, only one of the three residues proposed to reside in the solvent-exposed MMOB surface in the complex with MMOH is identical.

If we have identified the correct binding surface, then its overall characteristics are very similar in MMOBs from *Ms. trichosporium* OB3b and *Mc. capsulatus* (Bath). In particular, the putative interface surface of the *Mc. capsulatus* (Bath) is ringed by the same conserved set of negatively charged residues, and it contains many hydrophilic or charged residues. This suggests that ionic or hydrophilic forces also stabilize the complex with MMOH in this system. Indeed, the putative interface in the *Mc. capsulatus* (Bath) MMOB case contains an additional acidic residue (Asp 108) which may account for the somewhat lower component affinity in this case if a complementary charged residue in not present in MMOH (*24*, *47*).

Dynamics of the MMOB−MMOH Complex Formation Process. The intense fluorescence and sensitivity of the BADAN-labeled MMOB allows the rate constants for formation of the labeled MMOB−MMOH complex to be determined. The process exhibits fast and slow phases accounting for approximately 66% and 34% of the overall amplitude change, respectively. On the basis of the observation that only the fast phase exhibits dependence on MMOH concentration, it is argued above that the reaction occurs in two steps with an association step being the primary contributor to the fast phase. The association step is pH dependent and accounts for the observed pH dependence in the equilibrium K_D values. A similar linear concentration dependence for the association of MMOH and MMOB was observed on the basis of changes in Trp fluorescence in the *Mc. capsulatus* (Bath) system at pH 7.0 (*47*), but the rate constant in the forward direction was found to be 3 orders of magnitude smaller than that reported here. Also, only a single phase was observed by monitoring Trp fluorescence. A second phase was predicted to occur as part of a global conformational change linking the two active sites of the dimeric protomer structure of MMOH in order to account for the inhibition observed at high MMOB concentrations in steady-state experiments. However, the predicted rate constants for this change are far smaller than the turnover number for the system and, thus, are not part of the normal catalytic cycle. Although the forward and reverse rate constants for the second phase of the binding reaction we have observed here for the *Ms. trichosporium* OB3b system cannot be resolved, their sum is 2 orders of magnitude above the turnover number at 4 °C and comparable with the rate constant for the O_2 binding reaction to form the first peroxo intermediate in the reaction cycle (*9*). The reaction occurring during the second step of the binding process is unknown, but it would seem reasonable that it is a conformational change that ultimately results in the observed spectroscopic changes at the diiron cluster site of MMOH (*16*, *18*, *53*).

Relationship to the Mechanism. The results support many aspects of our proposal for the regulation of the mechanism of sMMO catalysis by MMOB (*25*, *27*, *39*). The formation of a strong complex between the MMOH and MMOB components is confirmed, and the change in affinity upon reduction of MMOH is directly demonstrated. This change clearly implies that a structural change in the MMOB−MMOH interface is energetically coupled to the oxidation state of the diiron cluster. Similarly, structural changes caused by association of MMOB with the oxidized form of MMOH are suggested by the kinetic properties of the apparent two-step association reaction. We have proposed that these conformational changes are related to creating a size-selective pathway for methane and O_2 into the MMOH active site mediated by sMMO residue T111 and other nearby residues. The proposed MMOB binding surface that emerges from these studies incorporates these residues in the interface. The nature of the putative size-selective pathway is unknown, but two possibilities for molecules the size of methane and O_2 are a physical pore or a region of increased mobility. In this regard, it is interesting to note that, whereas residue T111 is clearly sequestered and less mobile in the component complex, its mobility remains much higher than any other residue identified to be in the interface by the spin-labeling technique utilized here.

ACKNOWLEDGMENT

The authors acknowledge Dr. Gregory Hunter for technical advice in the area of fluorescence spectroscopy.

SUPPORTING INFORMATION AVAILABLE

A table showing the oligonucleotides used to construct the mutant MMOBs and five figures providing additional details for the experimental results. This material is available free of charge via the Internet at http://pubs.acs.org.

REFERENCES

1. Dalton, H. (1980) Oxidation of hydrocarbons by methane monooxygenase from a variety of microbes, *Adv. Appl. Microbiol. 26*, 71−87.
2. Woodland, M. P., and Dalton, H. (1984) Purification and characterization of component A of the methane monooxygenase from *Methylococcus capsulatus* (Bath), *J. Biol. Chem. 259*, 53−59.
3. Green, J., and Dalton, H. (1985) Protein B of soluble methane monooxygenase from *Methylococcus capsulatus* (Bath). A novel regulatory protein of enzyme activity, *J. Biol. Chem. 260*, 15795−15801.
4. Fox, B. G., Froland, W. A., Dege, J. E., and Lipscomb, J. D. (1989) Methane monooxygenase from *Methylosinus trichosporium* OB3b. Purification and properties of a three-component system with high specific activity from a type II methanotroph, *J. Biol. Chem. 264*, 10023−10033.
5. Wallar, B. J., and Lipscomb, J. D. (1996) Dioxygen activation by enzymes containing binuclear non-heme iron clusters, *Chem. Rev. 96*, 2625−2657.
6. Feig, A. L., and Lippard, S. J. (1994) Reactions of non-heme iron-(II) centers with dioxygen in biology and chemistry, *Chem. Rev. 94*, 759−805.
7. Merkx, M., Kopp, D. A., Sazinsky, M. H., Blazyk, J. L., Muller, J., and Lippard, S. J. (2001) Dioxygen activation and methane hydroxylation by soluble methane monooxygenase: a tale of two irons and three proteins, *Angew. Chem., Int. Ed. 40*, 2782−2807.
8. Brazeau, B. J., and Lipscomb, J. D. (2000) Electron transfer and radical forming reactions of methane monooxygenase, *Subcell. Biochem. 35*, 233−277.
9. Lee, S.-K., Nesheim, J. C., and Lipscomb, J. D. (1993) Transient intermediates of the methane monooxygenase catalytic cycle, *J. Biol. Chem. 268*, 21569−21577.
10. Rosenzweig, A. C., Frederick, C. A., Lippard, S. J., and Nordlund, P. (1993) Crystal structure of a bacterial non-haem iron hydroxylase that catalyses the biological oxidation of methane, *Nature 366*, 537−543.

11. Elango, N., Radhakrishnan, R., Froland, W. A., Wallar, B. J., Earhart, C. A., Lipscomb, J. D., and Ohlendorf, D. H. (1997) Crystal structure of the hydroxylase component of methane monooxygenase from *Methylosinus trichosporium* OB3b, *Protein Sci. 6*, 556−568.
12. Lindqvist, Y., Huang, W. J., Schneider, G., and Shanklin, J. (1996) Crystal structure of delta(9) stearoyl-acyl carrier protein desaturase from castor seed and its relationship to other diiron proteins, *EMBO J. 15*, 4081−4092.
13. Sazinsky, M. H., Bard, J., Di Donato, A., and Lippard, S. J. (2004) Crystal structure of the toluene/*o*-xylene monooxygenase hydroxylase from *Pseudomonas stutzeri* OX1. Insight into the substrate specificity, substrate channeling, and active site tuning of multicomponent monooxygenases, *J. Biol. Chem. 279*, 30600−30610.
14. Dyer, D. H., Lyle, K. S., Rayment, I., and Fox, B. G. (2005) X-ray structure of putative acyl-ACP desaturase DesA2 from *Mycobacterium tuberculosis* H37Rv, *Protein Sci. 14*, 1508−1517.
15. Froland, W. A., Andersson, K. K., Lee, S.-K., Liu, Y., and Lipscomb, J. D. (1992) Methane monooxygenase component B and reductase alter the regioselectivity of the hydroxylase component-catalyzed reactions. A novel role for protein−protein interactions in an oxygenase mechanism, *J. Biol. Chem. 267*, 17588−17597.
16. Fox, B. G., Liu, Y., Dege, J. E., and Lipscomb, J. D. (1991) Complex formation between the protein components of methane monooxygenase from *Methylosinus trichosporium* OB3b. Identification of sites of component interaction, *J. Biol. Chem. 266*, 540−550.
17. Davydov, A., Davydov, R., Gräslund, A., Lipscomb, J. D., and Andersson, K. K. (1997) Radiolytic reduction of methane monooxygenase dinuclear iron cluster at 77 K−EPR evidence for conformational change upon reduction or binding of component B to the diferric state, *J. Biol. Chem. 272*, 7022−7026.
18. Pulver, S. C., Froland, W. A., Lipscomb, J. D., and Solomon, E. I. (1997) Ligand field circular dichroism and magnetic circular dichroism studies of component B and substrate binding to the hydroxylase component of methane monooxygenase, *J. Am. Chem. Soc. 119*, 387−395.
19. Lee, S.-K., Fox, B. G., Froland, W. A., Lipscomb, J. D., and Münck, E. (1993) A transient intermediate of the methane monooxygenase catalytic cycle containing a $Fe^{IV}Fe^{IV}$ cluster, *J. Am. Chem. Soc. 115*, 6450−6451.
20. Liu, K. E., Valentine, A. M., Wang, D. L., Huynh, B. H., Edmondson, D. E., Salifoglou, A., and Lippard, S. J. (1995) Kinetic and spectroscopic characterization of intermediates and component interactions in reactions of methane monooxygenase from *Methylococcus capsulatus* (Bath), *J. Am. Chem. Soc. 117*, 10174−10185.
21. Brazeau, B. J., and Lipscomb, J. D. (2000) Kinetics and activation thermodynamics of methane monooxygenase compound Q formation and reaction with substrates, *Biochemistry 39*, 13503−13515.
22. Chang, S. L., Wallar, B. J., Lipscomb, J. D., and Mayo, K. H. (1999) Solution structure of component B from methane monooxygenase derived through heteronuclear NMR and molecular modeling, *Biochemistry 38*, 5799−5812.
23. Chang, S. L., Wallar, B. J., Lipscomb, J. D., and Mayo, K. H. (2001) Residues in *Methylosinus trichosporium* OB3b methane monooxygenase component B involved in molecular interactions with reduced- and oxidized-hydroxylase component: a role for the N-terminus, *Biochemistry 40*, 9539−9551.
24. Walters, K. J., Gassner, G. T., Lippard, S. J., and Wagner, G. (1999) Structure of the soluble methane monooxygenase regulatory protein B, *Proc. Natl. Acad. Sci. U.S.A. 96*, 7877−7882.
25. Wallar, B. J., and Lipscomb, J. D. (2001) Methane monooxygenase component B mutants alter the kinetics of steps throughout the catalytic cycle, *Biochemistry 40*, 2220−2233.
26. Nesheim, J. C., and Lipscomb, J. D. (1996) Large isotope effects in methane oxidation catalyzed by methane monooxygenase: evidence for C−H bond cleavage in a reaction cycle intermediate, *Biochemistry 35*, 10240−10247.
27. Brazeau, B. J., Wallar, B. J., and Lipscomb, J. D. (2001) Unmasking of deuterium kinetic isotope effects on the methane monooxygenase compound Q reaction by site-directed mutagenesis of component B, *J. Am. Chem. Soc. 123*, 10421−10422.
28. MacArthur, R., Sazinsky, M. H., Kuehne, H., Whittington, D. A., Lippard, S. J., and Brudvig, G. W. (2002) Component B binding to the soluble methane monooxygenase hydroxylase by saturation-recovery EPR spectroscopy of spin-labeled MMOB, *J. Am. Chem. Soc. 124*, 13392−13393.
29. Brazeau, B. J., Wallar, B. J., and Lipscomb, J. D. (2003) Effector proteins from $P450_{cam}$ and methane monooxygenase: lessons in tuning nature's powerful reagents, *Biochem. Biophys. Res. Commun. 312*, 143−148.
30. Hubbell, W. L., Cafiso, D. S., and Altenbach, C. (2000) Identifying conformational changes with site-directed spin labeling, *Nat. Struct. Biol. 7*, 735−739.
31. Altenbach, C., Froncisz, W., Hemker, R., Hassane, M., and Hubbell, W. L. (2005) Accessibility of nitroxide side chains: Absolute Heisenberg exchange rates from power saturation EPR, *Biophys. J. 89*, 2103-2112.
32. Fox, B. G., Froland, W. A., Jollie, D. R., and Lipscomb, J. D. (1990) Methane monooxygenase from *Methylosinus trichosporium* OB3b, *Methods Enzymol. 188*, 191−202.
33. Oh, K. J., Altenbach, C., Collier, R. J., and Hubbell, W. L. (2000) Site directed spin labeling of proteins. Applications to diphtheria toxin, *Methods Mol. Biol. 145*, 147−169.
34. Altenbach, C., Greenhalgh, D. A., Khorana, H. G., and Hubbell, W. L. (1994) A collision gradient method to determine the immersion depth of nitroxides in lipid bilayers: application to spin-labeled mutants of bacteriorhodopsin, *Proc. Natl. Acad. Sci. U.S.A. 91*, 1667−1671.
35. Kirby, T. L., Karim, C. B., and Thomas, D. D. (2004) Electron paramagnetic resonance reveals a large-scale conformational change in the cytoplasmic domain of phospholamban upon binding to the sarcoplasmic reticulum Ca-ATPase, *Biochemistry 43*, 5842−5852.
36. Nelson, W. D., Blakely, S. E., Nesmelov, Y. E., and Thomas, D. D. (2005) Site-directed spin labeling reveals a conformational switch in the phosphorylation domain of smooth muscle myosin, *Proc. Natl. Acad. Sci. U.S.A. 102*, 4000−4005.
37. Columbus, L., and Hubbell, W. L. (2004) Mapping backbone dynamics in solution with site-directed spin labeling: GCN4-58 bZip free and bound to DNA, *Biochemistry 43*, 7273−7287.
38. Lakowicz, J. R. (1999) Fluorescence anisotropy, in *Principles of Fluorescence Spectroscopy* (Lakowicz, J. R., Ed.) pp 291−320, Kluwer Academic/Plenum Publishers, New York.
39. Brazeau, B. J., and Lipscomb, J. D. (2003) Key amino acid residues in the regulation of soluble methane monooxygenase catalysis by component B, *Biochemistry 42*, 5618−5631.
40. Liu, Y., Nesheim, J. C., Lee, S.-K., and Lipscomb, J. D. (1995) Gating effects of component B on oxygen activation by the methane monooxygenase hydroxylase component, *J. Biol. Chem. 270*, 24662−24665.
41. Hiratsuka, T. (1999) ATP-induced opposite changes in the local environments around Cys697 (SH2) and Cys707 (SH1) of the myosin motor domain revealed by the PRODAN fluorescence, *J. Biol. Chem. 274*, 29156−29163.
42. Owenius, R., Österlund, M., Lindgren, M., Svensson, M., Olsen, O., Persson, E., Freskgård, P.-O., and Carllson, U. (2000) Properties of spin and fluorescent labels at a receptor−ligand interface, *Biophys. J. 77*, 2237−2250.
43. Mendelson, R. A., Morales, M. F., and Botts, J. (1973) Segmental flexibility of the S-1 moiety of myosin, *Biochemistry 12*, 2250−2255.
44. Osada, H., Nakanishi, M., Tsuboi, M., Kinosita, K., Jr., and Ikegami, A. (1984) Rotational dynamics of immunoglobulins with fluorescent haptens on a membrane surface, *Biochim. Biophys. Acta 773*, 321−324.
45. Callaghan, A. J., Smith, T. J., Slade, S. E., and Dalton, H. (2002) Residues near the N-terminus of protein B control autocatalytic proteolysis and the activity of soluble methane monooxygenase, *Eur. J. Biochem. 269*, 1835−1843.
46. Zhang, J., and Lipscomb, J., D. (2006) Role of the C-terminal region of the B component of *Methylosinus trichosporium* OB3b methane monooxygenase in the regulation of oxygen activation, *Biochemistry* (in press).
47. Gassner, G. T., and Lippard, S. J. (1999) Component interactions in the soluble methane monooxygenase system from *Methylococcus capsulatus* (Bath), *Biochemistry 38*, 12768−12785.
48. Paulsen, K. E., Liu, Y., Fox, B. G., Lipscomb, J. D., Münck, E., and Stankovich, M. T. (1994) Oxidation−reduction potentials of the methane monooxygenase hydroxylase component from *Methylosinus trichosporium* OB3b, *Biochemistry 33*, 713−722.
49. Brandstetter, H., Whittington, D. A., Lippard, S. J., and Frederick, C. A. (1999) Mutational and structural analyses of the regulatory

protein B of soluble methane monooxygenase from *Methylococcus capsulatus* (Bath), *Chem. Biol. 6*, 441−449.

50. Balendra, S., Lesieur, C., Smith, T. J., and Dalton, H. (2002) Positively charged amino acids are essential for electron transfer and protein−protein interactions in the soluble methane monooxygenase complex from *Methylococcus capsulatus* (Bath), *Biochemistry 41*, 2571−2579.
51. Stayton, P. S., Poulos, T. L., and Sligar, S. G. (1989) Putidaredoxin competitively inhibits cytochrome b_5-cytochrome P-450_{cam} association: a proposed molecular model for a cytochrome P-450_{cam} electron-transfer complex, *Biochemistry 28*, 8201−8205.
52. Stayton, P. S., and Sligar, S. G. (1990) The cytochrome P-450_{cam} binding surface as defined by site-directed mutagenesis and electrostatic modeling, *Biochemistry 29*, 7381−7386.
53. Hendrich, M. P., Münck, E., Fox, B. G., and Lipscomb, J. D. (1990) Integer-spin EPR studies of the fully reduced methane monooxygenase hydroxylase component, *J. Am. Chem. Soc. 112*, 5861−5865.

BI052256T